ADVANCED MATERIALS INTERFACES
www.advmatinterfaces.de

Peptoid-Loaded Microgels Self-Defensively Inhibit Staphylococcal Colonization of Titanium in a Model of Operating-Room Contamination

*Wenhan Zhao, Haoyu Wang, Xixi Xiao, Lauren De Stefano, Jordan Katz, Jennifer S. Lin, Annelise E. Barron, Thomas P. Schaer, Hongjun Wang, and Matthew Libera**

Bacterial contamination of an exposed implantable medical device by the atmosphere of an operating room (OR) is increasingly implicated as a cause of device-associated infection. Here, OR contamination is modeled in vitro using an aerosolizing system to spray small quantities of staphylococci onto titanium rods. Contaminated rods always manifest culturable bacteria. Self-assembly is used to create a self-defensive Ti surface that substantially enhances the rod's resistance to such contamination. Poly(acrylic acid) microgels are electrostatically deposited onto small Ti rods and subsequently loaded by complexation with a cationic antimicrobial peptoid (TM1). The microgels are visualized in situ by optical microscopy, and changes in microgel diameter indicate the loading state. These measurements show that TM1 can be quickly loaded from low-ionic-strength buffer and subsequently remained sequestered within the microgels for up to 4 weeks when soaked in phosphate buffered saline. TM1-loaded microgel-modified Ti surfaces are contaminated with aerosolized staphylococci, and subsequent assays indicate few or no culturable bacteria. In the absence of nutrients to enable metabolism, this finding suggests that bacteria trigger local TM1 release by contact transfer. The modified surfaces exhibit good in vitro cytocompatibility as manifested by the adhesion, spreading, and metabolic activity of human fetal osteoblasts.

1. Introduction

Despite the fact that the surgical operating room (OR) is commonly referred to as sterile or aseptic, the OR atmosphere in reality contains microbes from many sources. Among them are ventilation systems, shedding from clothing, sneezing or coughing by OR personnel, as well as pedestrian traffic both within and in/out of the room itself.[1] These airborne bacteria can accumulate on the surface of an implantable biomedical device once it is removed from its sterile package. Early measurements[2] reported a bacterial surface-accumulation rate of $\approx 3 \times 10^6$ CFU m^{-2} h^{-1}. Increased and improved practices of infection control have steadily reduced that rate. More recent studies report rates ranging from 10^3 to 10^4 CFU m^{-2} h^{-1}.[3] These rates suggest that devices are being implanted after they have been contaminated by hundreds or thousands of bacteria. Once implanted and exposed to favorable growth conditions within the body, a subset of these bacteria can develop into biofilms and lead to chronic device-associated infection.

Devices such as hip/knee prostheses,[4] heart valves,[5] pacemakers,[6] cochlear implants,[7] shunts,[8] surgical mesh,[9] sutures,[10] tissue-engineering constructs,[11] among many others, are susceptible to device-associated infection. The fact that the incidence of surgical site infection increases linearly with time in the OR is well established,[12] and there is strong consensus that intraoperative contamination is responsible for at least some device-associated infections.[13]

Self-defensive surfaces[14] represent an emerging and compelling strategy that may be able to inhibit bacterial colonization due to OR contamination. The term self-defensive

W. Zhao, X. Xiao, M. Libera
Department of Chemical Engineering and Materials Science
Stevens Institute of Technology
Hoboken, NJ 07030, USA
E-mail: mlibera@stevens.edu

H. Wang, H. Wang
Department of Biomedical Engineering
Stevens Institute of Technology
Hoboken, NJ 07030, USA

The ORCID identification number(s) for the author(s) of this article can be found under https://doi.org/10.1002/admi.202201662.

DOI: 10.1002/admi.202201662

L. De Stefano, J. Katz
Orthobond Corporation
Princeton, NJ 08852, USA

J. S. Lin, A. E. Barron
Department of Bioengineering
School of Medicine
Stanford University
Stanford, CA 94305, USA

T. P. Schaer
Department of Clinical Studies
New Bolton Center
School of Veterinary Medicine
University of Pennsylvania
Kennett Square, PA 19348, USA

was introduced by Boulmedais and co-workers[15] for the case of bacteria-triggered antimicrobial release. The mechanism is very different from a traditional method of elutive drug delivery. In contrast to elutive methods which continuously release antimicrobials whether they are needed or not, a self-defensive mechanism releases antimicrobial only when needed, releases it in very small amounts locally only where needed, and does not release it at all if there is no microbial challenge. Such surfaces have been developed by Sukhishvili and co-workers[16] who designed polyelectrolyte thin-film coatings to release antimicrobial in response to local pH changes. Cado et al.[15a] exploited microbial enzyme secretion and designed coatings that incorporate substrates for those particular enzymes so that local coating degradation would release an antimicrobial. Both approaches require bacterial metabolism to become active. However, prior to implantation, a contaminated device surface has no source of nutrients, and significant bacterial metabolism is unlikely. A self-defensive approach that relies on metabolism may thus not be appropriate for addressing OR contamination.

An alternate self-defensive mechanism referred to as contact transfer[14c] is well suited to the problem of OR contamination. We have shown[17] that bacterial contact alone, without metabolism, can drive responsive antimicrobial release from a polyelectrolyte microgel coating and transfer that antimicrobial to a challenging bacterium. This mechanism has been demonstrated using both gram-positive (*Staphylococci*) and gram-negative (*Escherichia coli*) bacteria. It has furthermore been demonstrated both in low (0.016 M) and higher (0.14 M) ionic-strength phosphate buffer at pH 7.4.[17] This transfer has been attributed to the fact that the bacterial envelope contains a high concentration of negative charge and hydrophobicity so that the complexation strength between the bacterium and the antimicrobial can be greater than that between the microgel and the antimicrobial. Bacterial proximity to the loaded microgel then creates a steep chemical-potential gradient to drive antimicrobial decomplexation from the microgel and its transfer to the bacterium. The magnitude of that gradient can be further influenced by ionic strength.[18]

Here we tested the hypothesis that a self-defensive synthetic surface can in the absence of nutrients for metabolism significantly inhibit bacterial colonization in an in vitro model of OR contamination. We electrostatically deposited microgels of poly(acrylic acid) (PAA) to form a sub-monolayer coating on either glass cover slips or titanium rods (as a model of orthopedic pins or screws) and, in a second self-assembly step, we loaded these with a cationic antimicrobial peptoid referred to as TM1 (also known as peptoid 1).[19] Peptoids are like peptides except that the side-groups are located on the amide nitrogen rather than on the α-carbon. In general, they are not proteolyzed,[20] thus improving biostability and reducing immunogenicity.[20a] In particular, TM1 is a helical and amphipathic 12 mer peptoid consisting of a trimer (N_{Lys}–N_{spe}–N_{spe}) repeated four times and terminated with a secondary amine group (**Figure 1**). Each of the four N_{Lys} moieties brings a primary amine group. These five amine groups are all protonated under physiological conditions, and TM1 thus has a net electrostatic charge of +5. In addition, each N_{spe} brings an aromatic moiety, which can contribute to complexation interactions.[21]

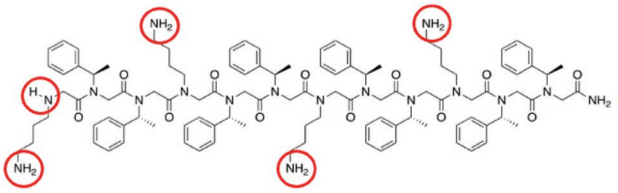

Figure 1. TM1 is a 12-mer antimicrobial peptoid with five positive charges at physiological pH (red circles).

In situ optical microscopy was used to follow the loading process by imaging the microgel deswelling during complexation with the TM1. Such imaging also assessed the ability of the TM1 to remain sequestered within the PAA microgels when exposed to physiologically relevant media. A digitally controlled aerosolizing system was used to spray well-defined quantities of staphylococci (either *Staphylococcus aureus* or *Staphylococcus epidermidis*) onto Ti rods. Subsequent in vitro assays of bacterial viability and osteoblast response showed that the TM1-loaded microgel-modified surfaces very effectively inhibit bacterial colonization while still preserving cytocompatability comparable to unmodified controls.

2. Experimental Section

2.1. Overview of the Surface Modification

The modification of the Ti rods by PAA microgels and the subsequent loading of these microgels required only a few self-assembly steps. The general procedure has been described previously.[22] In short, anionic PAA microgels were synthesized and electrostatically deposited onto titanium (Ti) rods. This deposition process produced a Ti surface modified by a sub-monolayer of PAA microgels. Small cationic antimicrobial molecules—the TM1 peptoid—were then loaded into these microgels by a second self-assembly step where the microgel-modified rod was immersed in an aqueous solution containing the TM1 peptoid. Because of electrostatic interactions, the peptoid diffused from the solution into the microgel and electrostatically complexed with the oppositely charged microgel network. This complexation process caused the microgels to deswell, a process that can be followed by in situ optical microscopy.

2.2. Microgel Synthesis, Loading, and Sequestration

PAA microgels were synthesized by thermally initiated, membrane emulsification. A precursor solution was mixed using 1.0 mL acrylic acid (Sigma), 0.47 g sodium hydroxide (NaOH, Sigma), 4 mL deionized (DI) water (Millipore type 1), 100 mg ammonium persulfate (Sigma), and 100 µL poly(ethylene glycol) diacrylate (M_n = 575 Da). This aqueous solution was forced via N_2 pressure (40 kPa) through a ceramic membrane (1.5 µm pore size (Shirasu Porous Glass) into a stirred (400 rpm) oil phase consisting of 2.56 g Span 80 and 160 mL paraffin oil. The resulting emulsion was then deoxygenated for 30 min by N_2 bubbling followed by heating to 70 °C and held

there for 4 h under continuous stirring (500 rpm). After cooling to room temperature, the paraffin oil was removed by centrifugation and the emulsion was resuspended first in cyclohexane two times, then in ethanol ten times, and finally in DI water ten times. The resulting PAA microgels were suspended in sterilized DI water and stored at 4 °C.

For in situ studies of microgel/antimicrobial interactions, a polydimethylsiloxane (PDMS) gasket was used to define 12 individual reaction chambers above a glass microscope slide. 6 mm diameter holes were punched from a cast sheet of cured PDMS (≈4 mm thickness). The punched gasket was then pressed onto a precleaned (3 min oxygen plasma) glass slide and annealed at 70 °C for 20 min. The volume of each glass-bottomed chamber was ≈100 µL. The glass surface within each chamber was primed with positively charged poly(allylamine hydrochloride) (PAH, Sigma, M_w = 17.5 kDa) using an aqueous solution of 0.2 mg PAH mL^{-1} for 1 h followed by gentle washing using DI water and then drying by flowing N_2 gas. A sub-monolayer of PAA microgels was then electrostatically deposited onto the primed glass surface by filling each chamber with a colloidal aqueous microgel suspension at room temperature and leaving it to soak for 30 min. These chambers were then rinsed with DI water and filled with 0.01 M phosphate buffer (pH 7.4, 4 mM NaH_2PO_4 and 6 mM Na_2HPO_4), $[Na^+]$ = 0.016 M) prior to subsequent antimicrobial loading.

TM1 (M_w = 1819 Da) was synthesized as previously described.[23] It was loaded by complexation within the microgels by replacing the buffer within a particular reaction chamber with a solution of 1 mg TM1 mL^{-1} in 0.01 M phosphate buffer. The loading process was followed by in situ time-resolved optical microscopy using an inverted microscope (Nikon, Eclipse Ti-E) equipped with a 14 bit CCD Camera (pco.pixelfly) and a CFI S Fluor ELWD 20 × objective lens (NA = 0.45, WD = 8.2–6.9 mm). During the first 10 min of loading, images were collected at 1-min intervals and then at 5-min intervals thereafter. After data acquisition, the time-resolved diameters of at least five different microgels were measured using ImageJ.[24] Each diameter was normalized using the initial diameter measured in TM1-free 0.01 M phosphate buffer.

The sequestration of the TM1 complexed within the microgels was again followed by in situ imaging. After loading, the TM1 solution was removed by gentle washing using DI water (three times). Each reaction chamber was then filled with either autoclaved 0.01 M phosphate buffer or autoclaved phosphate buffered saline (PBS, pH 7.4, ionic strength = 0.138 M). The buffer was replaced with fresh buffer daily for 28 days. Optical images of the same set of microgels were collected daily, and digital image analysis was used to measure the microgel diameter as a function of soaking time from at least five different microgels.

The amount of TM1 loaded into the microgels was quantified by UV absorption. Two aliquots of 10 µL of aqueous PAA microgel suspensions were prepared. One was allowed to fully dehydrate to measure the dry microgel weight. The other was added to 1 mL 0.01 M phosphate buffer containing 0.25 mg of TM1. After 60 min the loaded microgels were pelletized by centrifugation, and the UV adsorption (230 nm) of the supernatant was measured using a Synergy HT BioTek Spectrometer. The amount of loaded TM1 was then quantified by comparison with a calibration curve created using solutions of known TM1 concentrations in 0.01 M phosphate buffer. The microgel zeta potential was measured using a Malvern ZETA SIZER Nano series from aliqouts of microgels suspended in pure 0.01 M phosphate buffer and before/after TM1 loading.

2.3. OR Contamination Model

Commercially pure, surgical grade 1, titanium rods (1 cm length) were cut from wire (Temco RW0469) with an average diameter of 1.29 mm. These rods were used in anticipation of future in vivo experiments in a femoral infection model in a rat. The rods were rinsed twice with 70% ethanol, sonicated in ethanol (15 min), washed and sonicated in autoclaved DI water, and finally dried using flowing N_2 gas. The dried rods were then exposed to an oxygen plasma for 10 min. Further modifications were made to create four surfaces (**Table 1**). The PAH priming, electrostatic PAA microgel deposition, and the TM1 loading all followed the procedures described above for the glass substrates. The surfaces of each condition were imaged by scanning electron microcopy (SEM; Zeiss Auriga). TM1 loading for condition D was confirmed by exposing the modified pins to an aqueous solution of fluorescein isothiocyanate (FITC, Sigma) for 30 min in sterile DI water followed by repeated washing with DI water. The FITC-stained Ti-D rods were then imaged while hydrated using the Nikon Eclipse Ti-E inverted microscope with a C3 confocal attachment.

A digitally controlled aerosolizing system was used to contaminate the surfaces of rods in each of the four surface conditions with well-controlled quantities of bacteria. Details of the system configuration, operation, and properties have been described elsewhere.[25] The system is able to reproducibly spray well-defined bursts of aerosolized bacteria suspended in nutrient-free buffer onto test surfaces. Depending on the spray conditions, the density of sprayed bacteria is on the order of 10^2–10^3 cm^{-2} and can thus mimic the contamination conditions of a surgical theater. The experiments here used methicillin-sensitive *S. aureus* (MSSA, ATCC 29213) and *S. epidermidis* (ATCC 35984) obtained from the American Type Culture Collection (ATCC, Manassas, VA). For each set of experiments, a single bacterial colony was inoculated into 10 mL of Tryptic Soy Broth (TSB) and grown to stationary phase at 37 °C under gentle shaking for 18 h. The bacteria were pelleted by centrifugation and resuspended in sterile PBS twice to remove the TSB. After final pelleting, the bacteria were suspended in sterile PBS to an optical density (OD_{600}) of 0.0005A for MSSA and 0.0004A for *S. epidermidis*. These densities have been shown to produce contamination levels of ≈10^2 CFU cm^{-2}.[25] The solutions were kept at room temperature and used within 3 h of preparation. It

Table 1. Designations for four surface treatments.

Designation	Sample
Ti-A	Unmodified titanium rod
Ti-B	PAH-treated titanium rod (primed)
Ti-C	PAA-microgel-modified titanium rod (unloaded)
Ti-D	TM1-loaded PAA microgel-modified titanium rod

has been shown[25] that over 90% of the bacteria remain culturable under these preparation conditions.

Two sets of three Ti rods from each of the four surface-modification conditions were sprayed with 100 ms bursts of bacterial aerosol. One set was sprayed with MSSA, and the other was sprayed with *S. epidermidis*. The three rods from each set were sprayed simultaneously. After spraying, the samples were left to dry in air within a laminar-flow biosafety hood for 30 min. The extent of contamination was then quantified in terms of the numbers of i) loosely bound culturable bacteria and ii) strongly adhered culturable bacteria. Loosely bound bacteria were recovered by immersing each rod in 1.25 mL of sterile PBS followed by gentle vortexing. Three 250 µL aliquots of the buffer were then spread on separate tryptic soy agar (TSA) plates. Strongly adhered bacteria were assayed by gently washing each vortexed Ti rod using sterile PBS and then rolling each rod using flame-sterilized forceps over the surface of a TSA plate. Both sets of TSA plates were then cultured at 37 °C for 18 h. The number of colony-forming units (CFUs) was counted manually. The statistical significance of differences in bacterial colonization of the different surface-modification treatments was determined using a two-sided student *t*-test assuming unequal variances for the treated and control rods.

2.4. Cytocompatibility

Human fetal osteoblasts (hFOB, ATCC, VA) were cultured in a 1:1 mixture of Dulbecco's Modified Eagle's Medium (DMEM) and Ham's F12 Medium, containing 10% fetal bovine serum (Atlantic Biologicals) and 2.5 mM L-glutamine (without phenol red). Prior to use, the culture was maintained at 34 °C with 5% CO_2 and 95% humidity until 70–80% confluence. To achieve a homogeneous cell distribution on individual substrates (Ti rods or glass cover slips) and equally among multiple substrates, hFOB cells were seeded and cultured following a specific protocol. Briefly, the Ti rods and coverslips sampling each of the four surface-modification conditions (A-D) were sterilized using 70% ethanol and then washed for 2 min with sterile DI water (3×). All samples were again sterilized under UV irradiation for 20 min before cell seeding. Each rod was first seeded with 100 µL of hFOB cell suspension, and the cell-seeded rod was then incubated for 15 min (34 °C, 5% CO_2, and 95% humidity) to promote cell attachment. The seeded rod was then flipped over and exposed again to 100 µL of hFOB cell suspension to achieve a final seeding density of 2×10^4 cells cm^{-2}. Coverslips were seeded with 200 µL of hFOB cell suspension to a seeding density of 10^4 cells cm^{-2}. After 30 min of total incubation, all cell-seeded samples were transferred into a new 6-well plate for further cultivation. The culture medium was refreshed every 2 days.

The adhesion (1 day) and proliferation (4 day and 7 day) of hFOB cells on the rods were assessed using an MTS assay. Briefly, after 1, 4, and 7 days, the culture rods ($n = 3$ for each condition) were harvested, placed in a 12-well plate, and gently rinsed with cold PBS twice. Then, 1.4 mL of a mixture containing 400 µL MTS reagent (the assay kit was purchased from Promega, Madison, WI) and 1 mL culture medium was added each well. The plate was incubated for 2 h at 37 °C in 5% CO_2. 200 µL of supernatant from each sample was transferred to a 96-well plate. The absorbance at 490 nm was recorded using the BioTek Synergy microplate reader (BioTek Instruments, Inc., Vermont, USA). Statistically significant differences were assessed using a one-way *t*-test for the case where the Ti-A surface was used as the control and using an ANOVA test by Tukey's mean comparison ($p < 0.05$) for the case where the Ti-A, B, and C surfaces were used as controls.

The cell morphologies on Ti wires and coverslips were characterized after cultivation of 1, 4, and 7 days. The specimens were fixed with 4% (w/v) paraformaldehyde for 15 min and washed for 2 min with PBS (three times). Then, the samples were rinsed three times with 0.5% Triton X-100 and blocked with 3% (w/v) BSA to permeabilize the cell membranes. The cell nuclei were stained with 4′,6-diamidino-2-phenylindole (DAPI, Sigma, USA), and the cell skeletal filament actin (F-actin) was stained with Alexa Fluor 488-conjugated phalloidin. After staining, the samples were immersed in PBS and imaged while hydrated using a Nikon eclipse 80i epifluorescence microscope (Japan) and Zeiss LSM 880 confocal laser scanning microscope (Germany).

3. Results and Discussion

When hydrated in 0.01 M phosphate buffer at pH 7.4 and $[Na^+] = 0.016$ M, the as-synthesized PAA microgels have an average diameter of 6 ± 2 µm (Figure S1, Supporting Information). We have shown previously[21] that the carboxyl groups in the PAA are fully deprotonated under these conditions. They can thus complex with oppositely charged macroions such as the TM1 peptoid studied here. The fact that TM1 can be loaded into the PAA microgels by complexation is shown by **Figure 2**A. This plot follows the average microgel diameter during exposure to 0.01 M phosphate buffer with 1 mg mL^{-1} of TM1. The data are normalized to the average unloaded diameter (6.0 µm) at time $t = 0$ measured in TM1-free 0.01 M phosphate buffer. After 10 min, the normalized diameter decreases to ≈55%. In a separate experiment, measuring the decrease in TM1 concentration from the loading solution by UV absorption shows that 39.6 µg of dry microgel loads 206 µg of TM1. These values indicate a ratio of 4.8 acrylic acid groups for each molecule of TM1, which is very close to the stoichiometry of five −1 acid groups for each +5 TM1 molecule. The microgel zeta potential furthermore increased from a value of −33.5 ± 4.5 mV ($n = 6$) in the unloaded state ($t = 0$) to 3.6 ± 1.2 mV ($n = 6$) in the loaded state (both measurements made in 0.01 M phosphate buffer), again indicating charge neutralization due to TM1/PAA complexation.

Since device colonization is possible not only prior to implantation when the device is dry but also prior to surgical-site closure, an important question centers on whether the TM1 remains stably complexed within the PAA microgels when the device is in contact with physiological fluids. At a constant pH of 7.4, when the ionic strength is increased from $[Na^+] = 0.016$ M in the 0.01 M phosphate loading buffer to $[Na^+] = 0.14$ M typical of physiological conditions, the additional salt can shield the electrostatic pairing between amine groups on the TM1 and the acid groups within the PAA microgels. Such shielding, for example, leads to the burst release of colistin from PAA

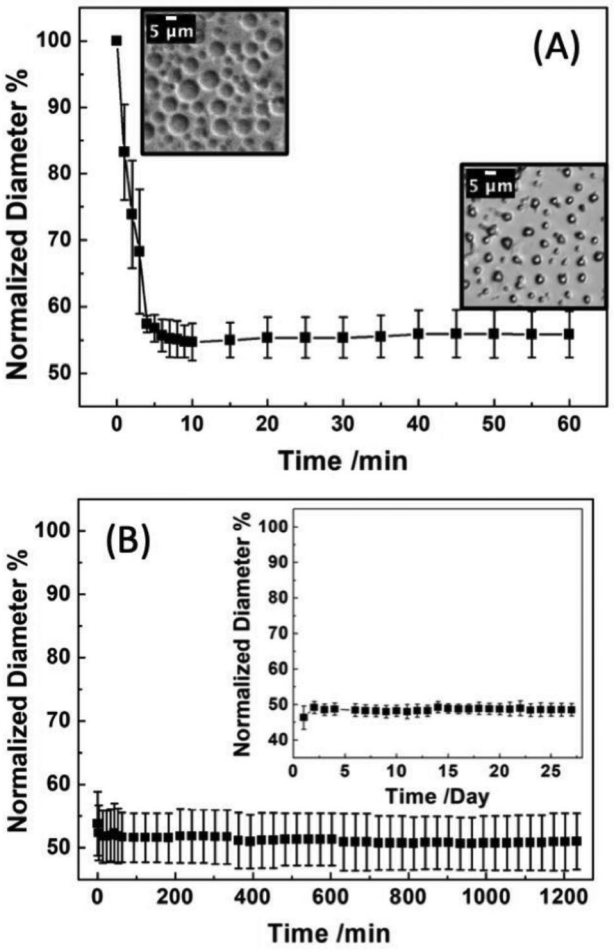

Figure 2. A) Time-resolved change in microgel diameter indicates TM1 loading (1 mg mL–1 TM1 in 0.01 M phosphate buffer) by complexation within PAA microgels. The inset optical images show the same set of hydrated microgels before/after loading. B) The lack of a diameter change indicates that the complexed TM1 remains sequestered within the PAA microgels when exposed to TM1-free PBS. Sequestration is maintained for 4 weeks (inset) with daily changes of PBS. Each data point/error bar represent the average/standard deviation from $n = 5$ measurements.

microgels.[17,21] The fact that Figure 2B shows no microgel diameter change when the loaded microgels are exposed to TM1-free PBS indicates stable TM1/PAA complexation. Similar experiments using flowing buffer with increasing concentrations of added NaCl indicate that a threshold $[Na^+] \approx 0.35$ M at pH 7.4 is needed to enable rapid release of the complexed TM1. This enhanced resistance to salting out in TM1/PAA relative to colistin/PAA is consistent with our recent observations that aromaticity enhances the complexation strength.[21] Exposure of TM1-loaded PAA microgels to serum-containing DMEM or to equine synovial fluid also does not induce changes in loaded microgel diameter and again indicates stable complexation in these more heterogeneous media (Figure S2, Supporting Information). The inset to Figure 2B furthermore indicates stable TM1/PAA complexation in PBS for periods as long as four weeks and, while not directly addressed here, may help enhance infection resistance post-operatively.

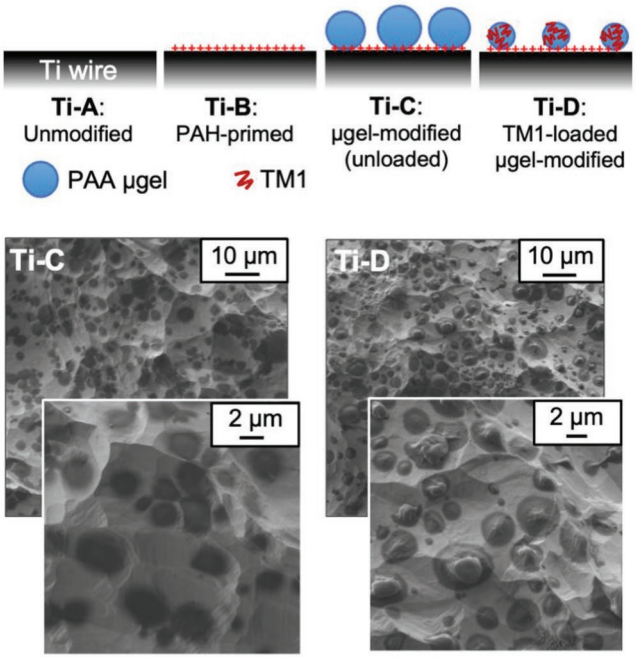

Figure 3. (Top) Schematic illustrations of four surface treatments applied to Ti rods. (Bottom) SEM images of the surfaces of rods modified with unloaded PAA microgels (bottom left) and TM1-loaded PAA microgels (bottom right). Images of all four surfaces are presented in Figure S3 of the Supporting Information.

Having developed a means to create TM1-loaded PAA-microgel modified surfaces by directed self-assembly, we studied the contamination resistance of Ti rods subjected to each of four different surface treatments. These are illustrated schematically in the top panel of **Figure 3**. The SEM images in Figure 3 bottom panel show the surface of rods modified with unloaded microgels (Ti-C) and with TM1-loaded microgels (Ti-D). The microgels form a sub-monolayer coating on the rough Ti surface with an inter-microgel spacing on the order of a few micrometers. The PAH-primed Ti surface is exposed between the microgels. The hydrated (unloaded) microgels comprise ≈97% water.[21] So, when dried for SEM imaging, they flatten and exhibit little topography. By contrast, the TM1-loaded microgels have substantially more mass and less hydration, and they exhibit very distinctive topography when dried.

To mimic intraoperative contamination by airborne bacteria, we sprayed three Ti rods sampling each of the four surface conditions with aerosols of 0.0067 M phosphate buffer (1× PBS with 0.0067 M PO_4, pH 7.0 to 7.2) containing either MSSA or *S. epidermidis*. After spraying, the rods were left to dry and then assayed to determine the number of culturable bacteria either loosely bound or strongly adhered to the Ti surface. We differentiate between these two cases mechanically by vortexing each rod in 0.0067 M phosphate buffer. Loosely bound bacteria were recovered in the buffer, and strongly adhered bacteria were recovered after vortexing by rolling the contaminated rod on an agar plate.

Figure 4 summarizes the results of these experiments. The images compare the TM1-loaded microgel-modified Ti-D to the unmodified control Ti-A for the case of MSSA contamination. The results are strikingly different. MSSA colonies

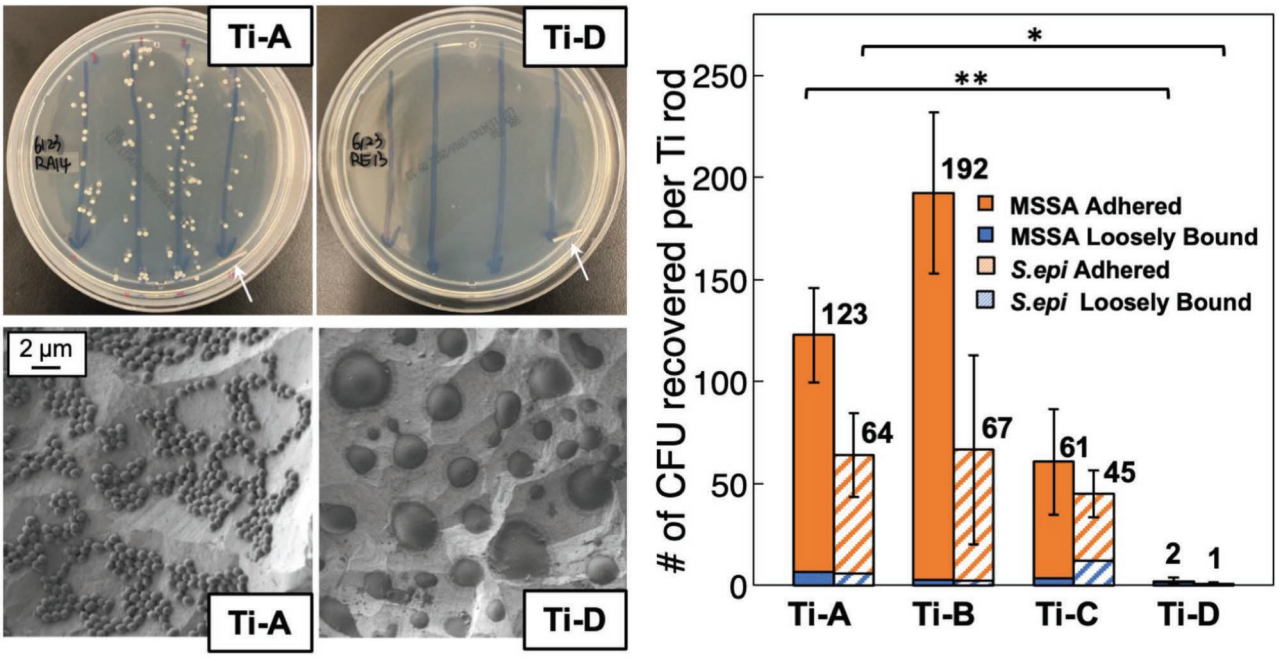

Figure 4. Assay of colonization resistance. The top left image shows the TSA plate assaying the culturable colonies on a Ti-A (unmodified) rod. The white arrow indicates the rod after rolling four times across the agar surface. The SEM image of the Ti-A rod (bottom left) after culture shows substantial MSSA colonization. The corresponding images for the Ti-D rod (TM1-loaded microgel modified) indicate no culturable colonies. The Ti-D SEM image shows that the loaded microgels remain intact on the rod surface, but MSSA are absent. Images for both MSSA and *S. epidermidis* contamination for all four (A-D) surface modifications are presented as Figures S4 and S5 of the Supporting Information. The right panel quantifies the total number of loosely bound and strongly adhered MSSA and *S. epidermidis* CGUs for each of the four conditions. The averages are indicated, and the error bars represent the standard deviation for $n = 3$ samples. * indicates $p < 0.05$, ** indicates $p < 0.005$.

(white dots) are evident in each of the four rolling paths for the Ti-A while none can be seen for the fully modified Ti-D. Recognizing that not all cultuarble bacteria are necessarily transferred from the rod (white arrows in the top images) to the agar, we imaged the rod surfaces via SEM. The lower left images of Figure 4 show extensive colonization of the unmodified Ti-A. However, no bacteria were found by SEM imaging of the Ti-D surface, though the microgels clearly remain present. The fact that the microgels remain loaded is reflected by their topography. The graph in Figure 4 quantifies the amount of loosely bound (solid blue) and strongly adhered (solid orange) MSSA for each of the four surface treatments. The cross-hatched data show the results of similar experiments using *S. epidermidis*. The trends are very similar. The PAH-primed rods (Ti-B) exhibit the highest degree of contamination, which is consistent with the fact that the PAH is positively charged at pH 7.4[26] and should attract bacteria, such as staphylococci, whose surface is negatively charged. Relative to the unmodified Ti-A, the (unloaded) microgel-modified Ti-C shows slightly fewer viable bacteria. This finding can be attributed to the fact that the microgels are less susceptible to colonization than the PAH-primed Ti surface, and the microgels block a fraction of the Ti surface.

Importantly, the number of culturable bacteria found on the TM1-loaded microgel-modified Ti-D samples is very small. In three trials we find an average of only 2 CFUs of MSSA and only 1 CFU of *S. epidermidis*. These few CFUs were all recovered from the buffer after vortexing the contaminated rod and thus correspond to loosely bound colonies. We found no CFUs from bacteria strongly adhered to the Ti-D rods.

Since the three control surfaces all became significantly colonized, we can assume that the Ti-D rods got similarly exposed to culturable bacteria due to the spray-contamination process. The fact that only a very small number of culturable colonies were subsequently found on the Ti-D rods indicates that the majority of these bacteria were killed by interaction with the surface. We note, however, that finding these dead bacteria by, for example, fluorescence imaging using a live/dead staining approach is experimentally challenging since the average density of sprayed bacteria is less than 2 per mm^2.

Neither the surface nor the medium (0.067 M phosphate buffer) in which the bacteria were suspended during the aerosolizing process provide nutrients, so we expect that the bacteria would undergo little or no metabolism on the surface. Hence, triggering TM1 release from the loaded microgels via local pH reduction[27] is unlikely. Instead, these findings support the concept of contact transfer where the local chemical potential of the TM1 is lower in the bacterial envelope than it is within the microgels,[14c,17] so that, when a bacterium comes within close proximity, some TM1 decomplexes from the microgel and recomplexes within the staphylococcal cell envelope. Such complexation interactions with bacteria have been extensively studied for a number of host-defense peptides and are attributed to the rich high concentration of anionic, hydrophobic, and aromatic moieties in the outer bacterial membranes.[28]

The fact that microgels, even when loaded, remain hydrophilic promotes opportunities for microgel-bacterium contact. If an aerosolized droplet impinges on a dry microgel-modified surface, water from that droplet will locally hydrate one or more microgels. As the overall droplet evaporates, the microgel(s) will be the most hydrophilic element of the surface and will be last to fully dry. We can anticipate that surface tension associated with the edge of the drying droplet will draw any bacteria it may contain to a microgel, and when droplet evaporation is complete those bacteria will be concentrated on or near a microgel.

We furthermore note that the in vitro model of OR contamination does not overwhelm the surface with bacteria as can be the case with in vivo infection models where a concentrated inoculum (e.g., 10^6–10^8 CFU mL^{-1}) is typically required in order to provoke infection in control animals such as rats and mice. The OR contamination model sprays low numbers of bacteria onto a rod surface. The probability of any particular microgel interacting with a bacterium is low. For that (much larger) subset of microgels that are unchallenged, the antimicrobial remains sequestered within these microgels (see the SEM image of the Ti-D rod in Figure 4) and is available to face a subsequent bacterial challenge should one occur. That much smaller subset of microgels that do interact with a bacterium present a high local concentration of antimicrobial, which the assays of Figure 4 indicate is sufficient to prevent surface colonization. The overall low number of bacteria involved in the contamination model again creates a situation where the probability of a second droplet landing on a TM1-depleted or partially depleted microgel is very low. Hence, microgel reloading, while in principle possible, is unnecessary.

We used cell morphology (imaging) and metabolic activity (MTS) to evaluate the short-term cytocompatibility of the various surfaces. In the case of microgel-modified surfaces, only a fraction of the surface is covered by microgels. The underlying PAH-primed Ti surface is exposed between adjacent microgels and, because the PAH is cationic, we can expect that this exposed surface becomes covered by negatively charged serum proteins (e.g., albumin, fibronectin, etc.) when exposed to serum-containing medium. We have shown previously that such microgel-modified surfaces remain highly compatible with both osteoblasts and macrophages.[17,29] We note that the unmodified Ti surface has an intrinsic roughness over lateral length scales on the order of 2–10 μm, and that this roughness is further perturbed by the addition of TM1-loaded microgels with characteristic dimensions on the order of 7 μm. Such surface topography has long been known to affect and, in many cases, enhance cell adhesion, spreading, and proliferation.[30]

Figure 5 shows the results of our cytocompatibility assays using human fetal osteoblasts. The cell metabolic activity was analyzed with MTS assay (Figure 5 top). The absorbance for each sample set was normalized to its value on day 1 in order to better assess the proliferation rate independent of the initial cell adhesion. The raw MTS absorption data are presented in Figure S6 of the Supporting Information. Importantly, the metabolic activity measured from the fully modified Ti-D samples was higher than that of the unmodified control samples (Ti-A). This indicates that the modified surface promotes the proliferation of hFOB cells. The imaging data in the bottom portion of Figure 5, while qualitative, indicate that the hFOB cells adhered

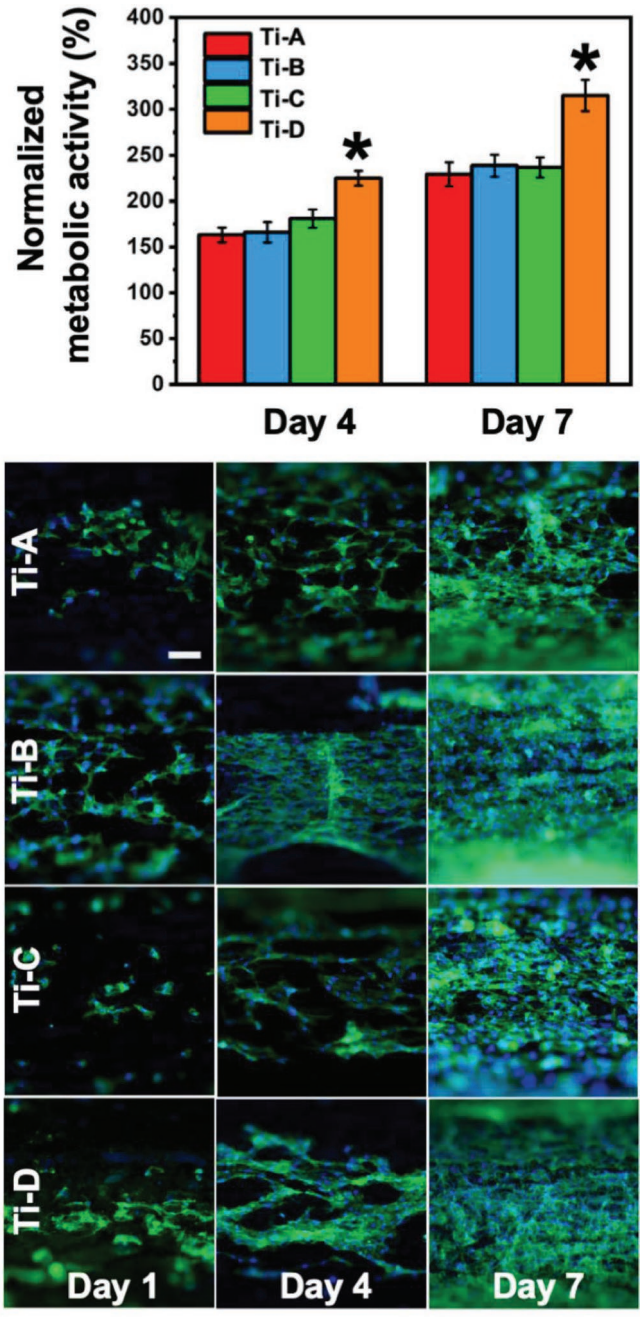

Figure 5. (Top) Metabolic activity of hFOB cells where the average for each surface treatment is normalized to its Day 1 value. The asterisk indicates a statistically significant difference (*t*-test with $p < 0.05$) between the fully modified Ti-D and the Ti-A unmodified control. (Bottom) Confocal fluorescence images (DAPI/Phalloidin staining) of hFOB cells grown on Ti rods with each of the four surface treatments (the scale bar is 100 μm).

to, spread, and proliferated on the various rods in a similar fashion. These results show that the TM1-loaded microgels are not only effective in inhibiting bacterial colononization but also do not cause noticeable cell incompatibilities, at least as observed with these short-term in vitro assays.

We avoided many of the imaging complications associated with the curved and rough surface of the Ti rods by using glass

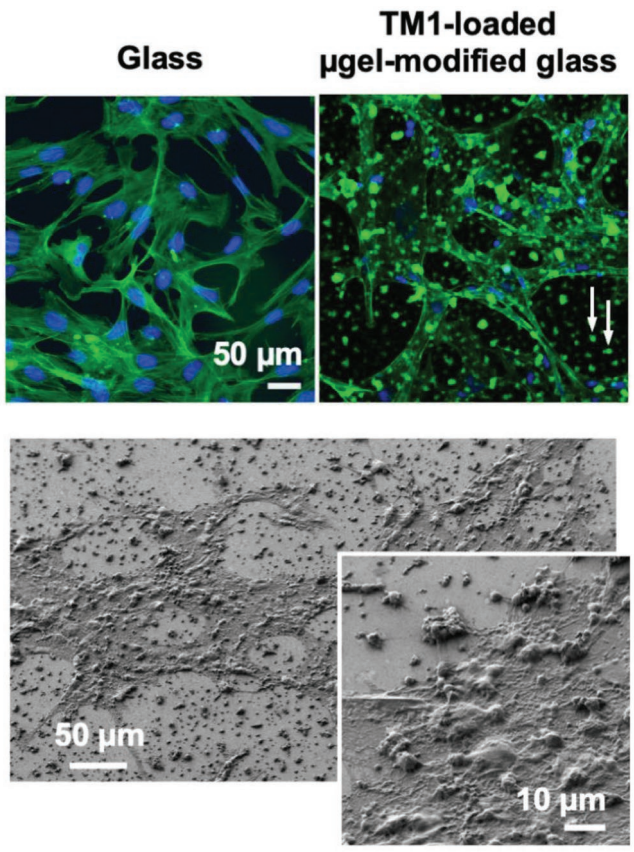

Figure 6. Confocal images of hFOB cells cultured on unmodified glass (top left) and TM1-loaded microgel-modified glass (top right) after 7 days of culture. The white arrows (top right) indicate autofluorescence from TM1-loaded microgels. Images of all four surfaces are presented in Figure S7 of the Supporting Information. The lower SEM images indicate that hFOB cells are able to spread over the TM1-loaded microgels.

substrates. The top images in **Figure 6** show that the morphologies of hFOB cells cultured for 7 days on unmodified glass and on TM1-loaded microgel-modified glass are comparable. The top right image also shows significant green contrast (see white arrows) distributed across the surface. We observe this fluorescence from TM1-loaded microgels only when the samples were dried after loading and later rehydrated for subsequent culturing experiments. We attribute this contrast to TM1 self-assembly within the microgels because of hydrophobic interactions, hydrogen bonds, and π–π stacking, which has recently been documented when TM1 self-assembles into helical bundles.[31] Importantly, the modified Ti rods (Ti-D) were processed identically—loaded, dried, and later rehydrated—which indicates that antimicrobial properties are preserved even if the TM1 forms such aggregated bundles. The autofluorescence not only indicates the location of the microgels but further indicates that the TM1 remains loaded within the microgels despite the presence of the hFOB cells. This finding is consistent with our previous results showing that culturing hFOB cells on PAA microgels loaded with the Sub5 antimicrobial peptide does not trigger AMP release.[17] SEM imaging (Figure 6 bottom) shows that the hFOB cells are able to grow right over the TM1-loaded microgels.

4. Conclusion

Exposure to the OR atmosphere between the time when a medical device is removed from its sterile package and the time when the wound site is fully closed can lead to device contamination by bacteria coming from the atmosphere. We have modeled that process using an aerosolizing system able to spray small quantities of bacteria onto titanium rods. Despite the fact that relatively low numbers of bacteria contaminate each rod, when exposed to culture medium, bacteria sprayed onto unmodified Ti rods develop into proliferating colonies. Our experiments show that Ti surfaces modified with polyanionic microgels loaded by complexation with a cationic antimicrobial peptoid, TM1, are able to almost entirely inhibit bacterial colony formation. Nutrients are unavailable to enable bacterial metabolism during the contamination process, indicating that the bacteria trigger local TM1 release by contact transfer rather than by local changes in pH. Because of the low numbers of contaminating bacteria, most of the loaded microgels are unchallenged during contamination, so their TM1 payload remains sequestered. However, neither the loaded peptoid nor the additional topography introduced by the microgels diminishes the cytocompatibility of the modified surfaces as assayed by in vitro experiments with human fetal osteoblasts. This surface-modification strategy thus suggests a promising approach with which to inhibit the intraoperative bacterial colonization of exposed biomedical devices due to contamination in the operating theater.

Supporting Information

Supporting Information is available from the Wiley Online Library or from the author.

Acknowledgements

The Stevens portion of this project was supported by the Army Research Office (Grant No. W911NF2010277) and by the National Science Foundation (DMR-1608406), which included supplemental funding to support Wenhan Zhao as an NSF Graduate Intern at Orthobond Corporation. A.E.B. and J.S.L. acknowledge funding from the U.S. Public Health Services (an NIH Pioneer award to Annelise Barron, NIH/NIA grant # 1DP1 OD029517-01). The authors thank Dr. Josefine Eilsø Nielsen for input on the manuscript. The authors thank Dr. Claudine Herlan and Dr. Natalia Molchanova for the TM1 synthesis at the Molecular Foundry, and the authors gratefully acknowledge the assistance of Dr. Michael Connolly there. Work at the Molecular Foundry was supported by the Office of Science, Office of Basic Energy Sciences, of the U.S. Department of Energy under Contract No. DE-AC02-05CH11231.

Conflict of Interest

The authors declare no conflict of interest.

Data Availability Statement

The data that support the findings of this study are available from the corresponding author upon reasonable request.

Keywords

antibacterials, drug delivery, implants, infection, microgel, self-assembly

Received: July 27, 2022
Published online:

[1] a) W. H. Organization, *Global Guidelines for the Prevention of Surgical Site Infection*, WHO, Geneva **2017**; b) R. R. W. Brady, J. Verran, N. N. Damani, A. P. Gibb, *J. Hosp. Infect.* **2009**, *71*, 295; c) D. Chauveaux, *Orthop. Traumatol.: Surg. Res.* **2015**, *101*, S77; d) T. T. Chow, X. Y. Yang, *J. Hosp. Infect.* **2004**, *56*, 85; e) K. Goswami, K. L. Stevenson, J. Parvizi, *Jt. Arthroplasty* **2020**, *35*, S2; f) S. M. McHugh, A. D. K. Hill, H. Humphreys, *Surgeon* **2015**, *13*, 52; g) J. Parvizi, S. Barnes, N. Shohat, C. E. Edmiston Jr., *Am. J. Infect. Control* **2017**, *45*, 1267; h) P. Weaving, F. Cox, S. Milton, *J. Perioper. Pract.* **2008**, *18*, 199.

[2] R. H. Fitzgerald Jr., *Arch. Surg.* **1979**, *114*, 772.

[3] a) M. Diab-Elschahawi, J. Berger, A. Blacky, O. Kimberger, R. Oguz, R. Kuelpmann, A. Kramer, O. Assadian, *Am. J. Infect. Control* **2011**, *39*, e25; b) C. Napoli, V. Marcotrigiano, M. T. Montagna, *BMC Public Health* **2012**, *12*, 594; c) C. Pasquarella, G. E. Sansebastiano, S. Ferretti, E. Saccani, M. Fanti, U. Moscato, G. Giannetti, S. Fornia, P. Cortellini, P. Vitali, C. Signorelli, *J. Hosp. Infect.* **2007**, *66*, 313.

[4] a) S. Kurtz, K. Ong, E. Lau, F. Mowat, M. Halpern, *J. Bone Jt. Surg., Ser. A* **2007**, *89*, 780; b) B. D. Springer, S. Cahue, C. D. Etkin, D. G. Lewallen, B. J. McGrory, *Arthroplasty Today* **2017**, *3*, 137; c) K. J. Bozic, *Am. Acad. Orthop. Surg.* **2018**.

[5] T. J. Cahill, B. D. Prendergast, *Lancet* **2016**, *387*, 882.

[6] M. Döring, S. Richter, G. Hindricks, *Dtsch. Arztebl. Int.* **2018**, *115*, 445.

[7] J. K.-L. Choong, S. J. O'Leary, in *Infections of the Ears, Nose, Throat, and Sinuses* (Eds: M. L. Durand, D. G. Deschler), Springer International Publishing AG (part of Springer Nature), Berlin **2018**.

[8] Y. Gutierrez-Murgas, J. N. Snowden, *J. Neuroimmunol.* **2014**, *276*, 1.

[9] M. Arnold, A. Kao, K. Gbozah, B. Heniford, V. Augenstein, *Int. J. Abdom. Wall Hernia Surg.* **2018**, *1*, 37.

[10] I. Ahmed, A. J. Boulton, S. Rizvi, W. Carlos, E. Dickenson, N. A. Smith, M. Reed, *BMJ Open* **2019**, *9*, e029727.

[11] R. Kuijer, E. J. P. Jansen, P. J. Emans, S. K. Bulstra, J. Riesle, J. Pieper, D. W. Grainger, H. J. Busscher, *Biomaterials* **2007**, *28*, 5148.

[12] a) H. K. Anis, N. Sodhi, A. K. Klika, M. A. Mont, W. K. Barsoum, C. A. Higuera, R. M. Molloy, *J. Arthroplasty* **2019**, *34*, S331; b) H. Cheng, B. P. H. Chen, I. M. Soleas, N. C. Ferko, C. G. Cameron, P. Hinoul, *Surg. Infect.* **2017**, *18*, 722; c) H. Cheng, J. W. Clymer, B. Po-Han Chen, B. Sadeghirad PhD, N. C. Ferko, C. G. Cameron, P. Hinoul, *J. Surg. Res.* **2018**, *229*, 134; d) B. Ravi, R. Jenkinson, S. O'Heireamhoin, P. C. Austin, S. Aktar, T. S. Leroux, M. Paterson, D. A. Redelmeier, *eClin. Med.* **2019**, *16*, 7410; e) R. E. Hubbard, I. A. Lang, D. J. Llewellyn, K. Rockwood, *J. Gerontol., Ser. A* **2010**, *65*, 377; f) H. White, F. Matheson, R. Moineddin, J. Dunn, R. Glazier, *Health Place* **2011**, *17*, 361.

[13] a) A. Baldini, K. Blevins, D. Del Gaizo, O. Enke, K. Goswami, W. Griffin, P. F. Indelli, T. Jennison, E. Kenanidis, P. Manner, R. Patel, T. Puhto, P. Sancheti, R. Sharma, R. Sharma, R. Shetty, R. Sorial, N. Talati, T. D. Tarity, K. Tetsworth, C. Topalis, E. Tsiridis, A. W-Dahl, M. Wilson, *J. Arthroplasty* **2019**, *34*, S97; b) C. L. Barnes, A. M. Cooper, J. Luque, J. Manghwani, W. Y. Matar, I. Panda, A. Rajgopal, S. Vaidya, O. Wakde, *J. Arthroplasty* **2019**, *34*, S175; c) A. M. Cooper, A. J. Shope, M. Javid, A. Parsa, M. A. Chinoy, J. Parvizi, *J. Bone Jt. Surg., Am.* **2019**, *101*, e133; d) J. Parvizi, T. Gehrke, M. A. Mont, J. J. Callaghan, *J. Arthroplasty* **2019**, *34*, S110.

[14] a) W. Ahmed, Z. Zhai, C. Gao, *Mater. Today Bio* **2019**, *2*, 100017; b) T. Wei, Q. Yu, H. Chen, *Adv. Healthcare Mater.* **2019**, *8*, 1801381; c) X. Xiao, W. Zhao, J. Liang, K. Sauer, M. Libera, *Colloids Surf., B* **2020**, *192*, 110989.

[15] a) G. Cado, R. Aslam, L. Séon, T. Garnier, R. Fabre, A. Parat, A. Chassepot, J. C. Voegel, B. Senger, F. Schneider, Y. Frère, L. Jierry, P. Schaaf, H. Kerdjoudj, M. H. Metz-Boutigue, F. Boulmedais, *Adv. Funct. Mater.* **2013**, *23*, 4801; b) L. Séon, P. Lavalle, P. Schaaf, F. Boulmedais, *Langmuir* **2015**, *31*, 12856.

[16] a) S. Pavlukhina, Y. Lu, A. Patimetha, M. Libera, S. Sukhishvili, *Biomacromolecules* **2010**, *11*, 3448; b) I. Zhuk, F. Jariwala, A. B. Attygalle, Y. Wu, M. Libera, S. A. Sukhishvili, *ACS Nano* **2014**, *8*, 7733.

[17] J. Liang, H. Wang, M. Libera, *Biomaterials* **2019**, *204*, 25.

[18] X. Xiao, J. Ji, H. Wang, S. Nanjia, H. Wang, M. Libera, *ACS Biomater. Sci. Eng.*, (Preprint), submitted Sep. **2022**.

[19] N. P. Chongsiriwatana, J. A. Patch, A. M. Czyzewski, M. T. Dohm, A. Ivankin, D. Gidalevitz, R. N. Zuckermann, A. E. Barron, *Proc. Natl. Acad. Sci. USA* **2008**, *105*, 2794.

[20] a) J. A. Gibbons, A. A. Hancock, C. R. Vitt, S. Knepper, S. A. Buckner, M. E. Brune, I. Milicic, J. F. Kerwin, L. S. Richter, E. W. Taylor, K. L. Spear, R. N. Zuckermann, D. C. Spellmeyer, R. A. Braeckman, W. H. Moos, *J. Pharmacol. Exp. Ther.* **1996**, *277*, 885; b) S. M. Miller, R. J. Simon, S. Ng, R. N. Zuckermann, J. M. Kerr, W. H. Moos, *Drug Dev. Res.* **1995**, *35*, 20; c) S. M. Miller, R. J. Simon, S. Ng, R. N. Zuckermann, J. M. Kerr, W. H. Moos, *Drug Dev. Res.* **1995**, *35*, 20.

[21] X. Xiao, J. Ji, W. Zhao, S. Nangia, M. Libera, *Macromolecules* **2022**, *55*, 1736.

[22] Y. Wu, J. Liang, Q. Wang, M. Libera, *MRS Online Proc. Libr.* **2013**, *1622*, 1.

[23] G. Diamond, N. Molchanova, C. Herlan, J. A. Fortkort, J. S. Lin, E. Figgins, N. Bopp, L. K. Ryan, D. Chung, R. S. Adcock, M. Sherman, A. E. Barron, *Pharmaceuticals* **2021**, *14*, 304.

[24] a) J. Schindelin, I. Arganda-Carreras, E. Frise, V. Kaynig, M. Longair, T. Pietzsch, S. Preibisch, C. Rueden, S. Saalfeld, B. Schmid, J.-Y. Tinevez, D. J. White, V. Hartenstein, K. Eliceiri, P. Tomancak, A. Cardona, *Nat. Methods* **2012**, *9*, 676; b) C. A. Schneider, W. S. Rasband, K. W. Eliceiri, *Nat. Methods* **2012**, *9*, 671.

[25] W. Zhao, M. Libera, M. Prysak, J. Katz, L. De Stefano, *J. Biomed. Mater. Res., Part B* **2022**, *10*, 1.

[26] J. Choi, M. F. Rubner, *Macromolecules* **2005**, *38*, 116.

[27] V. Albright, I. Zhuk, Y. Wang, V. Selin, B. van de Belt-Gritter, H. J. Busscher, H. C. van der Mei, S. A. Sukhishvili, *Acta Biomater.* **2017**, *61*, 66.

[28] a) N. Malanovic, K. Lohner, *Biochim. Biophys. Acta, Biomembr.* **2016**, *1858*, 936; b) N. Mookherjee, M. A. Anderson, H. P. Haagsman, D. J. Davidson, *Nat. Rev. Drug Discovery* **2020**, *19*, 311; c) W. C. Wimley, *ACS Chem. Biol.* **2010**, *5*, 905.

[29] a) Q. Wang, M. Libera, *Colloids Surf., B* **2014**, *118*, 202; b) Y. Wang, G. Subbiahdoss, J. Swartjes, H. C. van der Mei, H. J. Busscher, M. Libera, *Adv. Funct. Mater.* **2011**, *21*, 3916.

[30] a) C. C. Berry, G. Campbell, A. Spadiccino, M. Robertson, A. S. G. Curtis, *Biomaterials* **2004**, *25*, 5781; b) S. A. Biela, Y. Su, J. P. Spatz, R. Kemkemer, *Acta Biomater.* **2009**, *5*, 2460; c) D. Hoffman-Kim, J. A. Mitchel, R. V. Bellamkonda, *Annu. Rev. Biomed. Eng.* **2010**, *12*, 203; d) Y. Hu, J. O. You, J. Aizenberg, *ACS Appl. Mater. Interfaces* **2016**, *8*, 21939; e) M. Nikkhah, F. Edalat, S. Manoucheri, A. Khademhosseini, *Biomaterials* **2012**, *33*, 5230.

[31] J. E. Nielsen, M. A. Alford, D. B. Y. Yung, N. Molchanova, J. A. Fortkort, J. S. Lin, G. Diamond, R. E. W. Hancock, H. Jenssen, D. Pletzer, R. Lund, A. E. Barron, *ACS Infect. Dis.* **2022**, *8*, 533.

